Performance Investigation and Optimization of a S-type Turbine and Vortex-induced Vibration System

Yunrui Chen*

School of Energy and Power Engineering, Xi'an Jiaotong University, Xi'an 710049, Shaanxi, China
*Corresponding author: Yunrui Chen

Abstract: To develop deep-sea low-velocity ocean current energy, this paper proposes an array power generation system utilizing a coupled S-type turbine and vortex-induced vibration (VIV) device. A fluid-structure interaction calculation was developed using a combined simulation of Fluent and Matlab, and the relative positions of the two power generation devices were optimized using a genetic algorithm. The optimized results show that the array performs best at a horizontal distance of 1.5*D*–2.0*D* and a vertical distance of 1.5*D*, with the performance of the S-type turbine and VIV device improved by 12.5% and 45.3%, respectively, in the optimal case. Flow field analysis indicates that the performance improvement is due to the accelerated flow in the coupling region. This study provides a reference for array schemes with multiple underwater machines.

Keywords: Vortex-induced vibration; S-type turbine; fluid-structure interaction

1. Introduction

Deep-sea ocean current energy development and utilization have gradually become a research hotspot in recent years. Utilizing deep-sea power generation devices to convert the kinetic energy of deep-sea currents into electrical energy shows great potential for powering unmanned underwater vehicles, pre-positioned underwater weapons, and seabed monitoring equipment [1,2]. Therefore, developing in-situ power supply solutions for underwater equipment based on ocean current energy, especially low-velocity deep-sea ocean current energy [3], has become a current research focus.

Vortex-induced vibration (VIV) is a physical phenomenon widely present in nature. It occurs when a fluid flows past slender structures (oscillators), causing boundary layer separation and the alternating shedding of vortices on the upper and lower sides of a bluff body. This produces alternating lift forces that drive the bluff body and induce oscillation in the oscillator. VIV is a nonlinear, bidirectional fluid-structure interaction phenomenon. While it is generally considered detrimental to many structures, if the oscillator's structure and damping are properly designed, the resulting vibrations can be converted into mechanical power to drive a generator, making VIV a potential clean energy source. Bernitsas et al. at the University of Michigan [4-6] developed a vortex-induced vibration aquatic clean energy (VIVACE) converter, utilizing VIV to harness low-velocity water currents from rivers or oceans. Their results showed that the device could generate electricity in flow velocities as low as 0.25 m/s. Following this, VIVACE has been extensively studied by researchers worldwide. For instance, Lee et al. [7,8] experimentally tested the performance of VIVACE, using controllers to vary the internal damping of the generator to identify the optimal damping value. Ding et al. [9] improved VIVACE's energy conversion efficiency by altering the surface roughness of the oscillating cylinder, achieving a numerical efficiency peak of 37% and an experimental efficiency of 28%. Furthermore, the cross-sectional shape of the oscillator affects its efficiency and vortex-shedding patterns. Zhang et al. [10] investigated the performance of VIVACE with oscillators of various cross-sectional shapes, including triangular, quadrilateral, hexagonal, 24-sided, and circular. They found that cylindrical cross-sections yielded the highest efficiency, while triangular cross-sections were suitable for galloping power generation, and 24-sided cross-sections performed similarly to cylindrical ones. Current research on VIVACE's flow mechanisms, performance enhancement, and turbulence control is well-developed. To further increase the energy density of VIVACE devices, multi-oscillator array schemes, similar to clusters used in wind turbines, have garnered widespread attention.

The high-speed blocking flow regions between vibrators in a cluster and the flow coupling between them can enhance the power generation efficiency of the vibrators. The arrangement and coupling mechanisms of vibrators within a cluster are key areas of research. Sun et al. [11] experimentally tested the performance of a dual-vibrator system, showing that the efficiency of the dual-vibrator configuration can be increased by 2-6.69 times compared to a single-vibrator under compact arrangements. Kim and Bernitsas [12] tested an array of four cylindrical vibrators, finding that closely spaced vibrators can achieve an efficiency of 52.55% (88.6% of the Betz limit), attributed to overall spatial blockage and

local coupling of vibrators. They also found that a larger spacing between tandem rotors is necessary to minimize wake interference. Zhang et al. [13] conducted two-dimensional numerical simulations to study a cluster of four staggered cylindrical vibrators, focusing on the impact of vibrator spacing. The results showed that interference between tandem vibrators is more intense than between side-by-side vibrators. In terms of configuration optimization, Zhang et al. [14] optimized a V-shaped arrangement of cylindrical vibrators, where blockage effects and downstream vibrators suppress upstream vibrators operate in the energy recovery zone, resulting in an efficiency increase of 6.3%–8.4%.

In the context of VIVACE device clustering, achieving a more compact layout and higher efficiency is a primary goal. However, an overly compact layout can alter the flow field near upstream vibrators, potentially reducing efficiency. To address this, this paper proposes an arrangement with an upstream S-type turbine and downstream VIVACE vibrators. The advantage of this configuration is that the S-type turbine is less affected by downstream flow interference. Additionally, the forward blades of the S-type turbine accelerate the flow on the sides through their motion, thereby increasing the power generation of the vibrators.

Therefore, this study uses numerical computation methods to explore the complementary multi-machine combination of the S-type turbine and VIVACE, revealing the flow mechanisms and optimizing the optimal arrangement of the two devices, providing a reference for large arrays. The main tasks of this paper include: developing a two-way fluid-structure interaction simulation method based on Fluent and Matlab software; optimizing the arrangement of the dual machines; and analyzing the coupling mechanisms. These tasks aim to enhance the understanding and performance of large-scale array systems.

2. Method

2.1. Vortex-induced Vibration Physical Model

The design of the vortex-induced vibration ocean energy harvesting device in this study is consistent with conventional designs, as shown in Figure 1. It is simplified into a physical model that includes a spring and damper. Since the vortex-induced vibration oscillator is constrained in the direction perpendicular to the flow field velocity, only the motion of the cylinder in the y-direction, perpendicular to the flow velocity, is considered.

To study the motion characteristics of the vortex-induced vibration system, a dynamic analysis is first conducted to describe the relationship between the forces and motion (including velocity and acceleration) in the vibration system. This study falls under the first type of

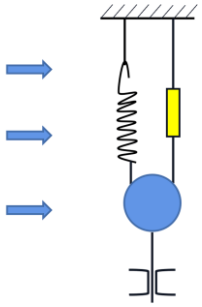

Figure 1. Simple physical model of VIVACE.

dynamics problem: determining motion from known forces. The cylinder is perpendicular to the incoming flow direction, which is defined as the x-axis, and the cylinder vibrates in the y-direction, perpendicular to the flow. This can be simplified as a mass-spring-damper single-degree-of-freedom vibration system. The differential equation of motion for the vortex-induced vibration cylinder can be expressed as:

$$\mathrm{m}\frac{d^2y}{dt^2} + \mathrm{C_{total}}\frac{\mathrm{dy}}{\mathrm{dt}} + \mathrm{Ky} = F_{fluid,y(t)} \tag{1}$$

where m is the mass of the vibrating cylinder, y is the displacement of the cylinder perpendicular to the flow direction, $\frac{d^2y}{dt^2}$ is the acceleration of the cylinder's oscillation, $\frac{dy}{dt}$ is the velocity of the cylinder's oscillation, C_{total} is the total damping of the system, which includes all forms of friction and damping generated by components like the motor, K is the spring sstiffness, $F_{fluid,y(t)}$ is the resultant fluid force on the cylinder in the perpendicular direction, which can be directly obtained using CFD methods in this study.

$$P_{FIM} = \frac{1}{T_{osc}}\int_0^{T_{osc}} C_{total}\left(\frac{dy}{dt}\right)^2 dt \tag{2}$$

2.2. Computational Domain and Boundary Conditions

The fluid domain of the VIV-S system comprising the S-type turbine and VIV oscillator is shown in Figure 2. In this configuration, the S-type turbine is positioned upstream, while the downstream VIV oscillator is located on the upper half-side of the S-type turbine, effectively utilizing the high-velocity flow region near the forward blades of the S-type turbine to enhance its power generation capacity. The S-type turbine is positioned at the origin of the coordinate system, with its center of rotation located 15 times the VIV diameter (15D) from the inlet and 25D from the outlet, ensuring full development of the wake. The cross-sectional width of the domain is 30D. The structural parameters of the VIV oscillator and the S-type turbine are provided in Table 1.

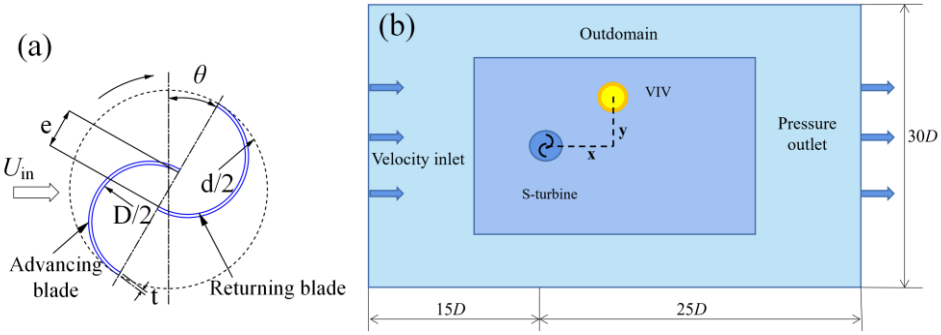

Figure 2. (a) Structural parameters of an S-type turbine; (b) computational domain.

Table 1. Table of structural parameters.

VIV		S-turbine	
Parameter	Value	Parameter	Value
Diameter, D_{VIV}	1 m	Diameter, D	1 m
Damping, C	350 kg/s	Overlap ratio, e	0.15
Stiffness, K	1200 N/m	Blade number	2
Mass, m	800 kg	Rotational speed	1 rad/s

The performance of the VIV-S system is evaluated using CFD numerical simulations. The boundary conditions for the fluid domain shown in Figure 2 are as follows:

1. Inlet: Velocity inlet boundary condition, with a direction perpendicular to the boundary and a magnitude of 0.5 m/s.

2. Outlet: Pressure outlet boundary condition, with a gauge pressure of 0 Pa.

3. Side-Wall: Symmetry boundary condition.

4. Cylinder-Wall (VIV oscillator and S-type turbine): No-slip boundary condition.

2.3. Mesh Distribution

In this study, ANSYS Meshing tool is used for mesh generation, choosing quadrilateral elements with progressively refined mesh from the outer to the inner regions. For the near-wall region mesh, specifically around the boundary layer of the cylinder, a refined boundary layer mesh is set up to accurately track the boundary layer flow and separation on the cylinder surface, and to precisely solve the near-wall viscous flow. The boundary layer mesh is set to twenty layers with a growth rate of 1.2. The k-ω SST turbulence model is selected, ensuring that the first layer mesh height satisfies a y+ value of 1. Figure 3 shows the mesh of the fluid domain and the refined regions.

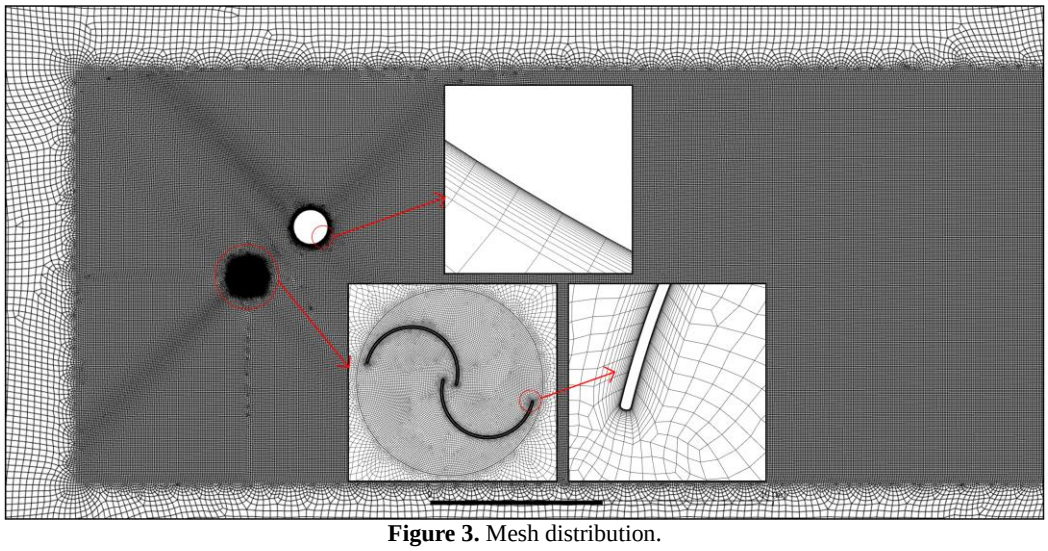

Figure 3. Mesh distribution.

In the numerical simulation of vortex-induced vibration (VIV), dynamic mesh technology is required to facilitate the transfer of force and displacement between the VIV oscillator and the fluid. This updates the displacement of the VIV oscillator at each time step. In this study, the smoothing method is chosen for the dynamic mesh technique. The principle behind this method is that the mesh in the fluid domain surrounding the VIV oscillator elastically deforms with the movement of the oscillator. The mesh compresses in the direction of the oscillator's movement and expands in the opposite direction.

2.4. Mesh and Time Step Independence Test

The simulations were conducted using five sets of meshes with different densities to analyze the impact of mesh density on the vortex-induced vibration (VIV) amplitude. Table 2 presents the comparison results of amplitude and frequency for mesh independence verification. From the data, it is visually evident that the

differences in the vibration response parameters of the VIV oscillator become negligible once the mesh count reaches 130,000. This indicates that further increasing the mesh count or density has an insignificant effect on the numerical simulation results.

Table 2. Mesh independence test.

Mesh	Amplitude(m)	Frequence(Hz)
50,000	0.0315	2.272
110,000	0.0310	2.274
130,000	0.0311	2.274
190,000	0.0311	2.274
240,000	0.0311	2.274

To study the impact of time step size on the simulation, five different time steps were selected for simulation. Table 3 presents the comparison of amplitude and frequency responses. It can be observed that when the time step size reaches 0.004 s, the amplitude error change is nearly zero, and the frequency error is less than 1%. To ensure both computational efficiency and accuracy, this study chooses 0.004 s as the simulation time step for subsequent simulations.

Table 3. Time step independence test.

Time step(s)	Amplitude (m)	Frequence（Hz）
0.008	0.0328	2.9204
0.006	0.0319	2.2218
0.004	0.0314	2.2488
0.003	0.0314	2.2615
0.002	0.0312	2.2743

3. Results and Discussion

3.1. Coupled Simulation

This study employs a numerical computation method using a coupled simulation of Matlab and Fluent, utilizing the UDP communication protocol to enable data exchange between Matlab and Fluent. Fluent is responsible for the flow field calculation and outputs the vertical fluid force acting VIV oscillator. Matlab receives the output data from Fluent and uses the Newmark-β method to solve the motion differential equations numerically. The resulting motion parameters, velocity, and displacement are then sent back to Fluent for the next time step's flow field calculation. The interaction method for the coupled simulation is illustrated in Figure 4.

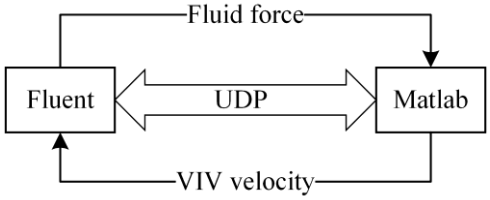

Figure 4. Simulation process of Fluent and Matlab.

3.2. Optimization of VIV-S System Arrangement

To maximize output power, the arrangement of the two power generation devices in Figure 2 was optimized using Latin hypercube sampling combined with a genetic algorithm to determine the optimal positions (x, y). Table 4 presents some of the optimization cases. The results indicate that the system achieves maximum power at (x, y) = (1892.5 mm, 1569.7 mm). At this configuration, the power output of the VIV oscillator is 17.15 W, and the power output of the S-type turbine is 18 W, which represents improvements of 45.3% and 12.5% compared to their isolated performances (with a single S-type turbine producing 16 W and a single VIV device producing 11.8 W). The enhancements are significant.

Furthermore, VIV-S arrays with arrangements close to the optimal positions (Case 1 and Case 7) also demonstrated good performance. Therefore, it can be concluded that the VIV-S array performs well at a longitudinal distance of 1.5*D*–2.0*D* and a vertical distance of 1.5*D*. The VIV oscillator benefits from the high-velocity region downstream of the S-type turbine, thereby enhancing its performance. However, when the vertical distance between the VIV oscillator and the S-type turbine is small (Cases 2, 4, 6, and 9), the VIV oscillator is exposed to the low kinetic energy wake region downstream of the S-type turbine, which adversely affects its power output.

Table 4. Experimental design.

Case	X (mm)	Y (mm)	VIV power(W)	S-turbine power(W)	Total power(W)
1	1827.7	1427.9	15.98	17.50	33.48
2	2034	259.6	0.69	16.57	17.26
3	1568.9	709.8	3.42	17.18	20.60
4	2416.7	242.4	0.72	16.61	17.33
5	2182.1	1090.6	8.59	16.68	25.27
6	1760	54.6	0.48	14.89	15.37
7	2016.8	1517.4	17.66	17.25	34.91
8	2863.1	598.8	2.47	16.48	18.95
9	2674.6	486.4	1.98	16.44	18.42
10	2378	979.4	7.70	16.25	23.95
11	2846.4	1576.5	13.61	16.28	29.89
12	1666.4	1254.1	9.66	18.35	28.01

3.3. Optimatation Results

To further analyze the performance of the VIV-S array under different installation positions of the two devices, the study examines a single VIV oscillator, Case 6, and the optimized case. Figures 5(a) and (b) show the vorticity contour and velocity contour of a single VIV oscillator, respectively. From Figure 5(a), it can be observed that as

the fluid flows around the cylinder, periodic shedding of clockwise and counterclockwise vortices occurs on both sides of the cylinder. The periodic forces generated by these vortices induce displacement in the cylinder. Due to the relatively low incoming flow velocity, this oscillation is classified as vortex-induced vibration (VIV). In Figure 5(b), periodic high-velocity regions extending downstream are visible on both sides of the cylinder. These high-velocity regions do not coincide with the vortex shedding zones. Such high-velocity regions, when acting on a downstream VIV oscillator, can enhance its power generation.

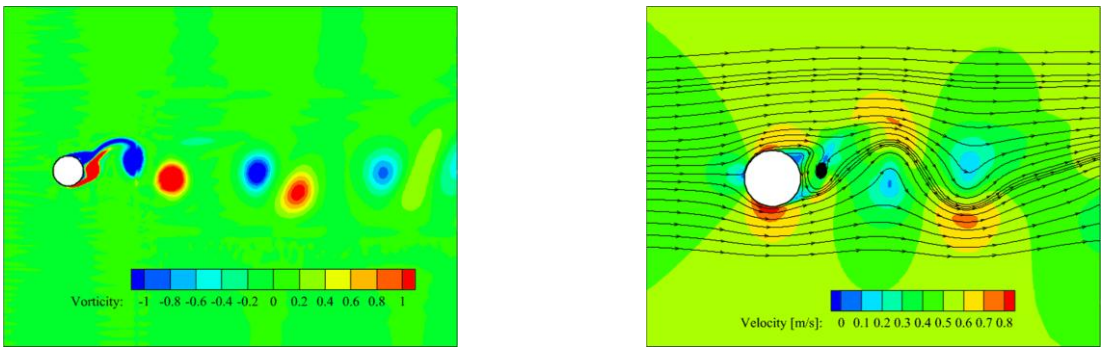

a. vorticity contour b. velocity contour

Figure 5. Vorticity and velocity contours of a single VIV.

Figures 6(a) and 6(b) show the vorticity and velocity contours for Case 6 from Table 4, which represents the configuration with the lowest performance for the downstream VIV oscillator. In this case, (x,y)=(1760mm,54.6mm), meaning the VIV oscillator is positioned near the center of the wake region behind the S-type turbine. From the vorticity contour in Figure 6(a), it is evident that the S-type turbine upstream periodically sheds vortices of opposite rotational directions from its sides. Since the VIV oscillator is almost parallel to the S-type turbine, the vortex shedding from the S-type turbine interferes with the vortex shedding from the VIV oscillator. Notably, the upstream vortices impact the front side of the VIV oscillator, and downstream of the VIV oscillator, the vortices from both devices merge. In the velocity contour shown in Figure 6(b), the flow velocity in front of the VIV oscillator in the wake region is extremely low. The vortices in the wake also affect the VIV oscillator, leading to very low power output. A clear flow separation region appears on the downstream side of the VIV oscillator. This is because the VIV oscillator, positioned in the wake, has a very low amplitude, causing the fluid flow around the cylinder to resemble "flow around a stationary cylinder" phenomenon.

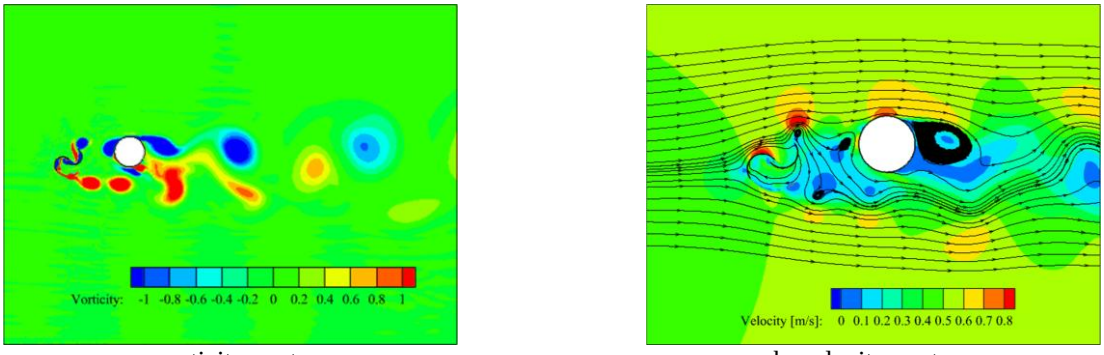

a. vorticity contour b. velocity contour

Figure 6. Vorticity and velocity contours of Case 6.

Figures 7(a) and (b) show the vorticity and velocity contours for the optimized case. Compared to Case 6, significant changes in the flow fields around the two devices are evident in the optimized case. In Figure 8(a), the vortex shedding from both the S-type turbine and the VIV oscillator exhibits slight interference in their respective high-speed flow regions. However, the size and downstream development direction of the vortices have slightly changed. Notably, the upstream vortices do not directly impact the VIV oscillator, and the vortices from the two devices do not merge. The velocity contour in Figure 7(b) reveals the presence of numerous high-speed rotating regions within the flow blockage area. These rotating regions increase the flow energy around the VIV oscillator, thereby enhancing its power output.

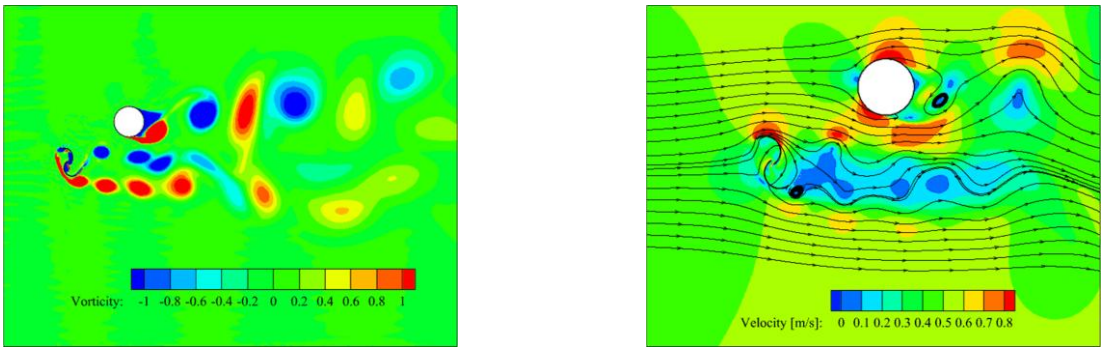

a. vorticity contour b. velocity contour

Figure 7. Vorticity and velocity contours of the optimal case.

The changes in the flow field lead to variations in the vibration frequency of the VIV oscillator. Figure 8 presents the vortex-induced vibration (VIV) frequency diagrams of the vertical force (Fy) and vertical amplitude (Y) for three types of cases. It can be observed that the frequency of the vertical force and amplitude is the same across the three cases, indicating that the VIV oscillators in all three cases exhibit vortex-induced vibration. However, the magnitude of the frequency and amplitude varies. The vibration frequency of a single VIV oscillator and the VIV oscillator in the optimized case is the same, at 0.112 Hz. In contrast, the VIV oscillator in Case 6 has a frequency of 0.106 Hz, which is slightly lower than that of the single VIV oscillator.

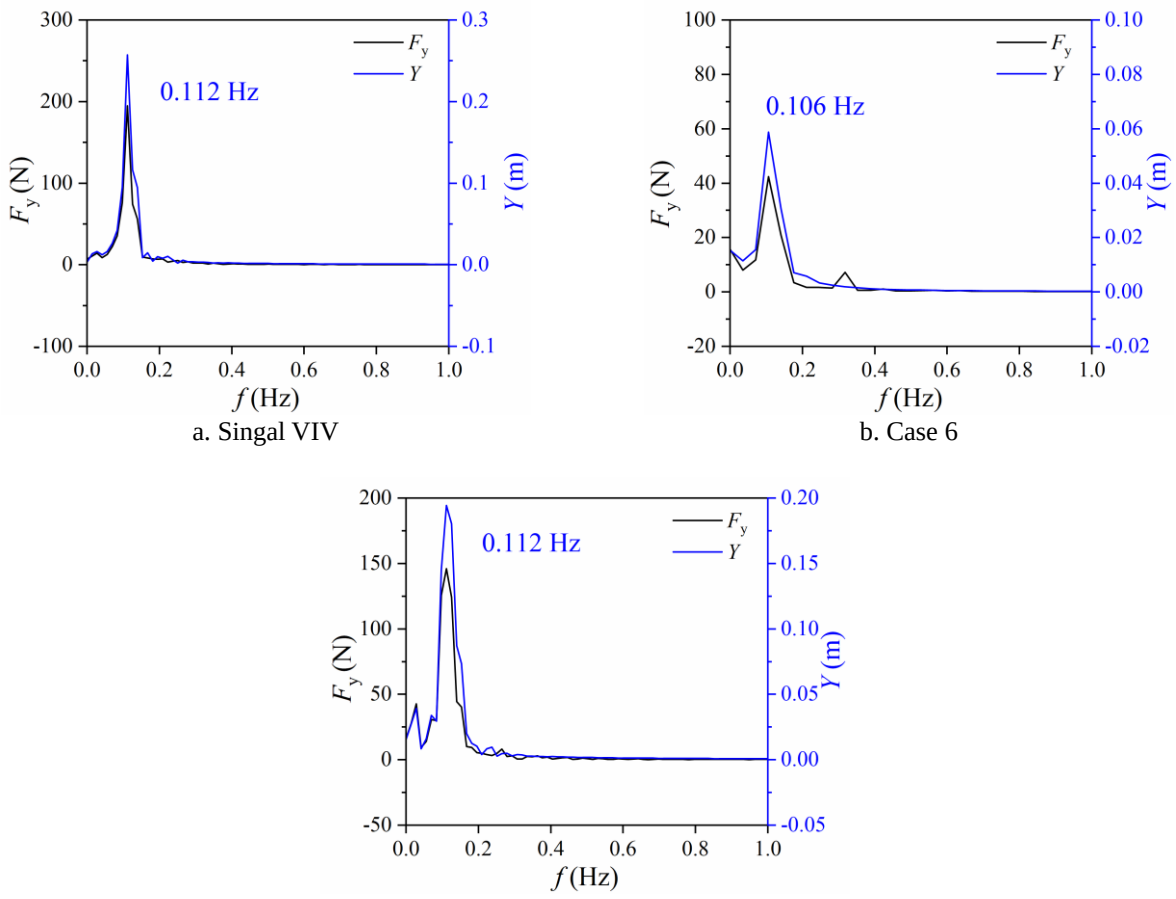

a. Singal VIV b. Case 6

c. Optimal case

Figure 8. Frequency spectrum of force and amplitude.

4. Conclusions

This study established a coupled simulation method for solving the VIV oscillator, utilizing data interaction between Fluent and Matlab software to achieve the simulation. A VIV-S array comprising a Savonius turbine and a VIV oscillator was proposed, and the arrangement within the array was optimized using a genetic algorithm. The following conclusions were drawn:

1. The VIV-S array consisting of the S-type turbine and VIV oscillator has significant development potential. A reasonable arrangement can greatly increase the power output of the downstream VIV oscillator without affecting the upstream S-type turbine. After optimization, the power

generation of the S-type turbine and VIV oscillator increased by 12.5% and 45.3%, respectively.

2. The coupling gain between the S-type turbine and VIV oscillator is attributed to the accelerated flow in the blockage area, with slight interference in their vortex shedding. However, when the VIV oscillator is in the wake of the S-type turbine, there is significant interference and vortex merging, which should be avoided during installation.

References

[1] D.Y. Zhang, P.H. Guo, Q. Hu, J.Y. Li, Parametric study and Multi-Objective optimization of a ductless Archimedes screw hydrokinetic Turbine: Experimental and numerical investigation, Energy Convers. Manag. 273 (2022) 116423. https://doi.org/10.1016/j.enconman.2022.116423.

[2] D.Y. Zhang, P.H. Guo, B. Xu, J.Y. Li, A deep-water in-situ power generation system based on chain-driven hydrokinetic turbine, J. Clean. Prod. 385 (2023) 135774. https://doi.org/10.1016/j.jclepro.2022.135774.

[3] B.M. Howe, Y. Chao, P. Arabshahi, S. Roy, T. McGinnis, A. Gray, A Smart Sensor Web for Ocean Observation: Fixed and Mobile Platforms, Integrated Acoustics, Satellites and Predictive Modeling, IEEE J. Sel. Top. Appl. Earth Obs. Remote Sens. 3 (2010) 507–521. https://doi.org/10.1109/JSTARS.2010.2052022.

[4] M.M. Bernitsas, Y. Ben-Simon, K. Raghavan, E.M.H. Garcia, The VIVACE Converter: Model Tests at High Damping and Reynolds Number Around 105, J. Offshore Mech. Arct. Eng. 131 (2008). https://doi.org/10.1115/1.2979796.

[5] M.M. Bernitsas, K. Raghavan, Y. Ben-Simon, E.M.H. Garcia, VIVACE (Vortex Induced Vibration Aquatic Clean Energy): A New Concept in Generation of Clean and Renewable Energy From Fluid Flow, J. Offshore Mech. Arct. Eng. 130 (2008). https://doi.org/10.1115/1.2957913.

[6] M.M. Bernitsas, K. Raghavan, G. Duchene, Induced Separation and Vorticity Using Roughness in VIV of Circular Cylinders at 8×103 < Re < 2.0×105, in: American Society of Mechanical Engineers Digital Collection, 2009: pp. 993–999. https://doi.org/10.1115/OMAE2008-58023.

[7] J.H. Lee, N. Xiros, M.M. Bernitsas, Virtual damper–spring system for VIV experiments and hydrokinetic energy conversion, Ocean Eng. 38 (2011) 732–747. https://doi.org/10.1016/j.oceaneng.2010.12.014.

[8] J.H. Lee, M.M. Bernitsas, High-damping, high-Reynolds VIV tests for energy harnessing using the VIVACE converter, Ocean Eng. 38 (2011) 1697–1712. https://doi.org/10.1016/j.oceaneng.2011.06.007.

[9] L. Ding, L. Zhang, M.M. Bernitsas, C.-C. Chang, Numerical simulation and experimental validation for energy harvesting of single-cylinder VIVACE converter with passive turbulence control, Renew. Energy 85 (2016) 1246–1259. https://doi.org/10.1016/j.renene.2015.07.088.

[10] B. Zhang, B. Song, Z. Mao, B. Li, M. Gu, Hydrokinetic energy harnessing by spring-mounted oscillators in FIM with different cross sections: From triangle to circle, Energy 189 (2019) 116249. https://doi.org/10.1016/j.energy.2019.116249.

[11] H. Sun, C. Ma, E.S. Kim, G. Nowakowski, E. Mauer, M.M. Bernitsas, Hydrokinetic energy conversion by two rough tandem-cylinders in flow induced motions: Effect of spacing and stiffness, Renew. Energy 107 (2017) 61–80. https://doi.org/10.1016/j.renene.2017.01.043.

[12] E.S. Kim, M.M. Bernitsas, Performance prediction of horizontal hydrokinetic energy converter using multiple-cylinder synergy in flow induced motion, Appl. Energy 170 (2016) 92–100. https://doi.org/10.1016/j.apenergy.2016.02.116.

[13] B. Zhang, Z. Mao, B. Song, W. Tian, W. Ding, Numerical investigation on VIV energy harvesting of four cylinders in close staggered formation, Ocean Eng. 165 (2018) 55–68. https://doi.org/10.1016/j.oceaneng.2018.07.042.

[14] B. Zhang, Z. Mao, L. Wang, S. Fu, W. Ding, A novel V-shaped layout method for VIV hydrokinetic energy converters inspired by geese flying in a V-Formation, Energy 230 (2021) 120811. https://doi.org/10.1016/j.energy.2021.120811.